ACS APPLIED MATERIALS & INTERFACES

Research Article

www.acsami.org

Preparation of Nitrogen-Doped TiO_2/Graphene Nanohybrids and Application as Counter Electrode for Dye-Sensitized Solar Cells

Rui Wang,[†] Qingduan Wu,[‡] Yun Lu,[#] Hongwei Liu,[§] Yanzhi Xia,[†] Jingquan Liu,*[,†] Dongjiang Yang,*[,†,§] Ziyang Huo,*[,§] and Xiangdong Yao*[,§]

[†]College of Chemistry, Chemical and Environmental Engineering; Laboratory of Fiber Materials and Modern Textile, the Growing Base for State Key Laboratory, Qingdao University, Qingdao 266071, China

[‡]China National Academy of Nanotechnology & Engineering, Teda, Tianjin 300457, China

[§]Queensland Micro- and Nanotechnology Centre (QMNC), Griffith University, Nathan, Brisbane, Queensland 4111, Australia

[#]Material Science and Engineering College, Key Laboratory of Bio-based Material Science and Technology, Ministry of Education, Northeast Forestry University, Harbin 150040, P.R. China

ABSTRACT: The preparation of nitrogen-doped TiO_2/graphene nanohybrids and their application as counter electrode for dye-sensitized solar cell (DSSC) are presented. These nanohybrids are prepared by self-assembly of pyrene modified $H_2Ti_3O_7$ nanosheets and graphene in aqueous medium via $\pi-\pi$ stacking interactions, followed by thermal calcination at different temperatures in ammonia atmosphere to afford nitrogen-doped TiO_2/graphene nanohybrids. $H_2Ti_3O_7$ nanosheets were synthesized from $TiOSO_4{\cdot}xH_2O$ by a hydrothermal reaction at 150 °C for 48 h. The microstructure of the obtained mixed-phase nanohybrids was characterized by transmission electron microscopy (TEM), X-ray diffraction (XRD), X-ray photoelectron spectroscopy (XPS), and Fourier transforms infrared spectroscopy (FTIR). Moreover, the performances of the as-prepared nanohybrids as counter electrode materials for DSSC was investigated, and the results indicated that the nanohybrids prepared at higher nitridation temperature would lead to higher short-circuit current density than those prepared at lower nitridation temperature, indicating that it can be utilized as a low-cost alternative to Pt for DSSCs and other applications.

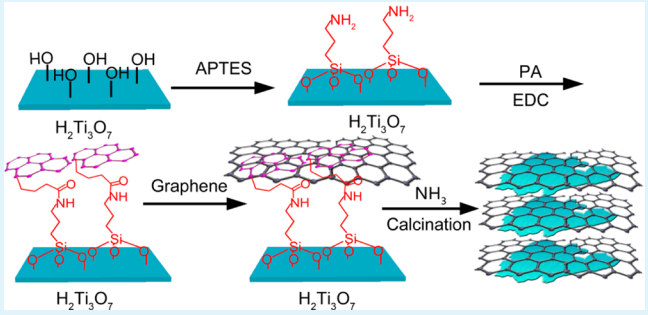

KEYWORDS: *nitrogen-doped TiO_2, graphene, graphene nanohybrids, $\pi-\pi$ stacking, counter electrode, dye-sensitized solar cells*

1. INTRODUCTION

Out of the considerations for natural resource depletion and environmental issue, dye-sensitized solar cells (DSSC), as one of photovoltaic solar devices directly converting sunlight into electricity by electrochemical reactions, have attracted widespread attentions because of their low-cost, simple manufacturing process, relatively high energy conversion efficiency, and low toxicity to the environment.[1] In general, DSSC consists of three main components: a photoactive working electrode (WE) containing light-absorbing dye molecules bound on a semiconductor material, a counter electrode (CE) capable of collecting electrons from external circuit and catalyzing the reduction of triiodide ions in electrolyte, and a redox active electrolyte couple (I^-/I^{3-}) to connect the electrodes.[2] The photoanode and electrolyte have been extensively explored in much of the literature,[3−5] whereas the counter electrodes have not received wide attention so far. Efficient counter electrodes can reduce inner energy loss in DSSC and hence generate higher current density and fill factors.[6] Traditionally, the noble metal platinum is preferredly selected as counter electrode material in DSSCs because of its high electrocatalytic activity, outstanding electrical conductivity and good stability. However, Pt is expensive (one of the most expensive materials available) and easily corroded in the presence of electrolyte solution. Moreover, Pt can be converted into PtI_4 in the presence of I^-/I^{3-} redox couple, which will severely affect the device stability.[7,8] For the above-mentioned reasons, some more stable and cheaper materials such as various conductive polymers,[6,8−10] carbon nanotubes,[7,11−14] carbons,[15,16] graphite,[17] graphene quantum,[18] inorganic semiconductor materials,[19−23] and biphase composites[6,24−30] have been explored as cost-effective alternatives to replace Pt for DSSCs counter electrodes .

It is observed that some transition metal nitrides exhibit noble-metal-like behaviors toward the reduction of triiodide ions because of their similar electronic structures and hence can be utilized as low-cost and platinum-free counter electrode in DSSCs. Highly ordered titanium nitrides (TiN), with high

Received: November 19, 2013
Accepted: January 10, 2014
Published: January 10, 2014

electrical and thermal conductivity, high catalytic activity as well as low-temperature superconductivity, are excellent alternatives as counter electrodes for DSSCs. However, TiN electrode alone has low fill factor and unsatisfied electrical conductivity because of the electron transport barrier across the boundaries of TiN nanocrystallites; therefore, some conducting paths should be introduced into TiN to improve its electrical conductivity and capacity. Graphene and carbon nanotubes (CNTs) are undoubtedly attractive and promising building blocks to intensify the electrode performance of TiN because they can construct a fast transport network for electron transfer, improve electrical conductivity and capacitance, and create highly active sites on the electron pathway. Wen et al. have successfully prepared a titanium nitride/graphene hybrid demonstrated comparable catalytic ability for triiodide ions reduction with Pt counter electrode in DSSCs.[31] Likewise, the network of TiN-CNTs were also prepared by anchoring TiN nanoparticles on the CNTs and found that the composite can provide high electrical conductivity and superior electrocatalytical activity as counter electrode materials.[32]

In the previous research, composite materials of pure TiN and carbon have been prepared as counter electrodes for DSSCs. As the precursor of TiN, TiO_2 can be completely transformed into TiN by carefully controlling the operating condition. Likewise, a bifunctional structure (TiO_2−TiN) can also be obtained by solely adjusting the calcination temperature. It can be expected that such a bifunctional structure might exhibit synergetic effect for better electrode performance. Compared with the pure TiN, no research utilizing this nitrogen-doped TiO_2 as counter electrodes in DSSCs has been reported before. In this work, for the first time, we present a facile, efficient method to prepare nitrogen-doped TiO_2/graphene hybrid by either covalent or noncovalent $\pi-\pi$ stacking methodologies, which involved in three steps: (1) preparing titanic hydroxide ($H_2Ti_3O_7$) nanosheets, (2) modifying the surface of titanic hydroxide with (3-aminopropyl) triethoxysilane (APTES) and 1-pyrenebutyric acid (PA) respectively, (3) attaching graphene by $\pi-\pi$ stacking, followed by calcinations at 570 and 700 °C in an ammonia atmosphere for 1 h (Scheme 1), and finally, the resulting hybrids are directly utilized as highly efficient counter electrode materials for DSSCs.[33,34]

Scheme 1. Schematic Illustration for the Surface Modification of $H_2Ti_3O_7$ with (3-Aminopropyl) Triethoxysilane (APTES) and 1-Pyrenebutyric Acid (PA), Followed by the Attachment of Graphene and Nitridation at Different Temperatures

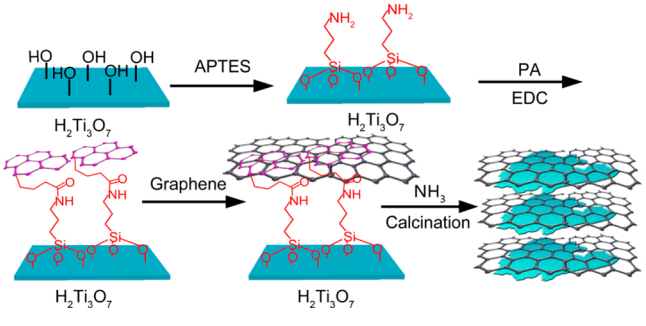

2. EXPERIMENTAL SECTION

2.1. Synthesis of $H_2Ti_3O_7$ Nanosheets. $H_2Ti_3O_7$ nanosheets were synthesized according to the method suggested by Yang and Liu.[35,36] NaOH pellets and hydrochloric acid (both are AR grade from Aldrich) and $TiOSO_4{\cdot}xH_2O$ (98%, from Fluka) were used in the synthesis. First, titanate nanosheets were prepared via a hydrothermal reaction between a concentrated NaOH solution and titanium salt. In brief, 3.6 g of $TiOSO_4{\cdot}xH_2O$ was dissolved in 27 mL of water and stirred by sonication until the mixture became clear. Afterward, 13 mL of 15 M NaOH solution was added into the resultant $TiOSO_4$ solution while stirring. The mixture (white suspension) was then transferred into 100 mL Teflon-lined stainless steel autoclave and kept at 150 °C for 48 h to yield titanate precipitate. The precipitate was recovered by suction filtration, washed with deionized water to remove the excess NaOH, and then exchanged with H^+ using a 0.1 M HCl solution to produce $H_2Ti_3O_7$ nanosheets. Finally, $H_2Ti_3O_7$ nanosheets were thoroughly rinsed using distilled water until pH ∼7 was reached. The obtained nanosheets were dried at 80 °C for 12 h prior to the further applications.

2.2. Surface Modification of $H_2Ti_3O_7$ Nanosheets. In brief, 1 g of $H_2Ti_3O_7$ nanosheets and 10 g of (3-aminopropyl) triethoxysilane (APTES) (99%, from Qufu Wanda) were dispersed and refluxed in 100 mL of toluene at 100 °C for 6 h. The resulting pale yellow product was carefully washed using toluene and then dried at 80 °C for 12 h. Afterward, 0.8 g of the above-obtained product reacted with 0.4 g of 1-pyrenebutyric acid (PA, 97%, from Sigma Aldrich) in 50 mL of tetrahydrofuran (THF, from Tianjin Fuyu) for 12 h, using 0.4 g of 1-ethyl-3-(3-dimethylaminopropyl) carbodiimide hydrochloride (EDC·HCl, 98.5%, from Adamas Regent Co. Ltd.) as coupling agent. The pyrene surface-modified $H_2Ti_3O_7$ nanosheets were centrifuged and dried at 40 °C for 12 h.

2.3. Preparation of Graphene. Graphene was prepared by the reduction of graphene oxide (GO), which was synthesized from natural graphite powder (KNGTM-150) using the method of Hummers and Offeman.[37,38] The chemically converted graphene was obtained by the reduction of GO at 95 °C in a hydrazine solution at pH 10.[39]

2.4. Preparation of Nitrided TiO_2/Graphene Hierarchical Nanostructure. In a typical synthesis of nitrogen-doped TiO_2/graphene hybrids, 144 mg of graphene was dispersed in 1000 mL of water and sonicated at 40 kHz for 4 h to afford a homogeneous suspension, followed by the addition of 336 mg of surface-modified $H_2Ti_3O_7$. The resulting mixture was stirred for 12 h and filtered to afford the expected product, which was dried at 40 °C for 12 h. The as-prepared composites were nitrided in a tubular furnace at 570 °C (N-TA/G-570) and 700 °C (N-TA/G-700) for 1 h in ammonia atmosphere, respectively, to afford the nitrogen-doped TiO_2/graphene hybrids.

2.5. Characterization. The micromorphologies and energy-dispersive X-ray spectroscopy (EDX) of the samples were obtained on a JSM-7600F field emission scanning electron microscope (SEM). Transmission electron microscopy (TEM) images were obtained at 200 kV on a JEM-1200EX (Japan). Samples were dropped on a carbon film supported on a Cu grid. Fourier transform infrared (FT-IR) spectroscopy measurements were carried out with a Nicolet Nexus 5700 (Thermo Electron Corporation, USA) using KBr pellets. The specific surface area Brunauer−Emmett−Teller (BET) was measured using a Micromeritics TriStar surface area and porosity analyzer by nitrogen absorption. The compositions of samples were analyzed by an X-ray diffractometer (DX-2700, Haoyuan Corporation, China). X-ray photoelectron spectroscopy (XPS) data were obtained on an ESCALab220i-XL electron spectrometer (VG Scientific, West Sussex, U.K.) using 300 W Al Kα radiation. The base pressure was about 3×10^{-9} Mbar. The binding energies were referenced to the C1s line at 284.8 eV from adventitious carbon. DSSCs were illuminated by a solar simulator (CHF-XM500, Beijing Trusttech Co. Ltd.) under 100 mW cm^{-2} (calibrated by a standard silicon solar cell) irradiation. Both the photocurrent−voltage characteristic curves of the DSSCs under simulated sunlight and the electrochemical impedance spectroscopy

dx.doi.org/10.1021/am405231p | ACS Appl. Mater. Interfaces 2014, 6, 2118−2124

(EIS) of the counter electrodes were recorded using an IM6ex (Zahner, Germany) electrochemical workstation. The frequency range was from 100 kHz to 100 mHz with an AC modulation signal of 20 mV and bias DC voltage of −0.60 V.

3. RESULTS AND DISCUSSION

3.1. Morphology of the Composites. The structural details of the nitrogen-doped TiO_2/graphene hybrids were investigated by transmission electron microscopy (TEM). The morphology of the $H_2Ti_3O_7$/graphene hybrids nitrided at 570 °C is shown in Figure 1A−E. It can be observed from the TEM

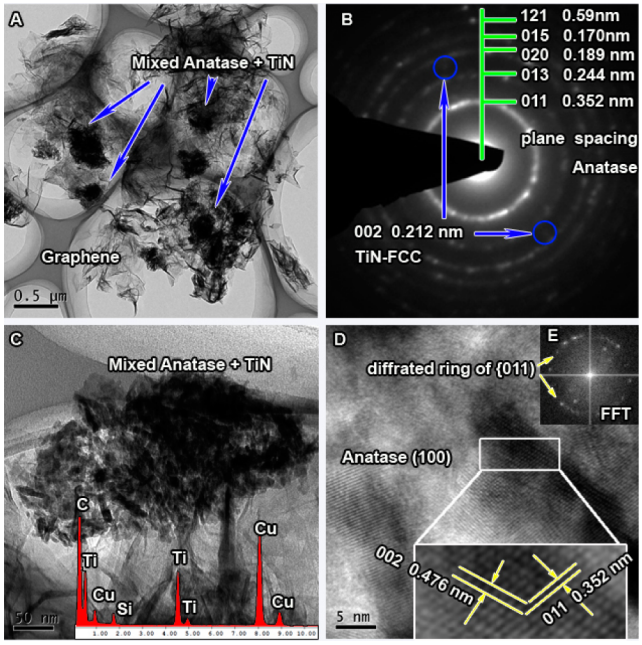

Figure 1. $H_2Ti_3O_7$/graphene nanohybrids calcined at 570 °C in NH_3 atmosphere for 1 h: (A) TEM image; (B) SAED pattern; (C) EDX; (D) HRTEM image; (E) fast Fourier transformation image.

bright-field image (Figure 1A) that the mixed TiO_2−TiN aggregates (black color) are closely embedded with the ultrathin graphene sheets (transparent gray color), indicating the successful preparation of nitrogen-doped TiO_2/graphene hybrid. Selected area electron diffraction rings corresponding to Panel A are shown in Figure 1B, where the rings could be attributed to the anatase phase and TiN phase. Please note that most of the rings are originated from the anatase while the ring with planar distance of 0.212 nm could be indexed with (002) plane of TiN phase (face centered cubic). TEM bright field image of another area with higher magnification and energy dispersion spectrum profile indicate the existence of three elements: C, Ti, and Cu (Figure 1C). High-resolution TEM image from titania aggregate area taken under <100] direction (The sign "<100]" means it is possible any one of the directions [100] and [010]). The inset at the bottom is the enlarged image from the selected area, which gives clear lattice fringes of planes (002) and (011) of anatase (Figure 1D). Fast Fourier transformation image in panel E corresponds with panel D, from which the (011) diffraction spot is sharp and white in intensity.

TEM micrographs of the $H_2Ti_3O_7$/graphene hybrids nitrided at 700 °C are shown in Figure 2. Among them, high-resolution TEM image from titania aggregate area taken under the <010] direction (The sign "<010]" means any one of the directions

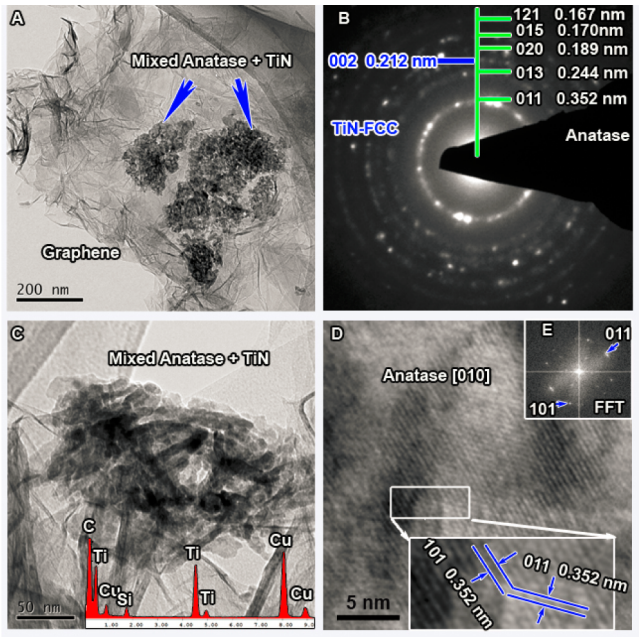

Figure 2. $H_2Ti_3O_7$/graphene nanohybrids calcined at 700 °C in NH_3 atmosphere for 1 h: (A) TEM image; (B) SAED pattern; (C) EDX; (D) HRTEM image; (E) fast Fourier transformation image.

[100] and [010] is possible) (Figure 2D). The inset at the bottom is the enlarged image from the selected area and gives clear lattice fringes of planes (101) and (011) of anatase. Fast Fourier transformation in panel E corresponds with panel D, from which the (101) diffraction spot is sharp and white in intensity (Figure 2E).

3.2. XRD Analysis. As shown in Figure 3, the nitrogen-doped TiO_2/graphene crystallographic structure could also be

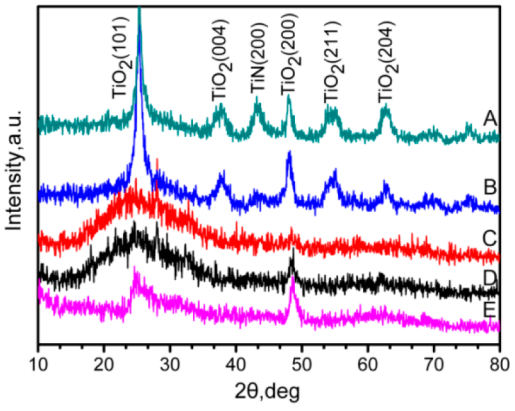

Figure 3. XRD patterns of (A) $H_2Ti_3O_7$/ graphene calcined at 700 °C in NH_3 atmosphere for 1 h; (B) $H_2Ti_3O_7$/graphene calcined at 570 °C in NH_3 atmosphere for 1 h; (C) $H_2Ti_3O_7$/graphene in NH_3 for 1 h at ambient temperature; (D) $H_2Ti_3O_7$/graphene; (E) $H_2Ti_3O_7$.

confirmed by X-ray diffraction. After calcination at 570 and 700 °C for 1 h in ammonia atmosphere, diffraction peaks indexed to the cubic anatase phase (JCPDS 21−1272) corresponding to (101), (004), (200), (211), and (204) and the face-centered cubic (FCC) TiN (JCPDS 87−0633) corresponding to (200) can be clearly observed (curve A, B), indicating the successful nitrogen doping to the TiO_2/graphene nanohybrids. Under these temperature conditions, the nitridation partly occurred on

dx.doi.org/10.1021/am405231p | ACS Appl. Mater. Interfaces 2014, 6, 2118−2124

the surface of the TiO_2 while the bulk phase remains untouched. The TiN diffraction peak of the hybrids obtained at 570 °C is weaker than that obtained at 700 °C because of the lower nitrogen content, which is in good agreement with the results of XPS. In a similar research by Jiang and Li, the TiO_2 nanotube arrays could be completely transformed into pure TiN after nitridation at 800 °C for 1 h in an ammonia atmosphere.[32,34] Obviously, the nitridation temperature is a key factor in phase transmission.

3.3. FTIR Analysis. The stepwise prepared $H_2Ti_3O_7$/graphene, and after N doping in the presence of NH_3 at ambient temperature, 570 and 700 °C, respectively were characterized using FTIR spectroscopy. The spectrum of $H_2Ti_3O_7$/graphene is shown in Figure 4A. The broad band at

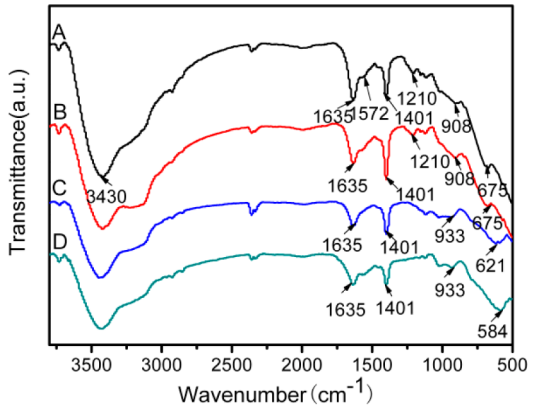

Figure 4. FTIR spectra: (A) $H_2Ti_3O_7$/graphene; (B) in NH_3 for 1 h at ambient temperature; (C) calcined at 570 °C in NH_3 atmosphere for 1 h ; (D) calcined at 700 °C in NH_3 atmosphere for 1 h.

3600−3100 cm^{-1} is attributed to O−H stretching. The weak peak centered at 1635 cm^{-1} is attributed to an O−H bending vibration, due to the structural OH groups and the adsorbed water. The C═C stretching band of the aromatic groups at 1572 cm^{-1} is also observed in the spectrum. The peakat 1401 cm^{-1} is attributed to Ti−O bending vibration and the peak at 1210 cm^{-1} should be contributed to the stretching of N−C (N−C═O). The signals in the range 400−1250 cm^{-1} are the characteristic of the formation of O−Ti−O lattice. Curve B in Figure 4 is for the sample in the presence of NH_3 for 1 h at ambient temperature. The only difference from curve A is the appearance of the peak at 3250−3000 cm^{-1} which corresponds to the N−H stretching vibrations, indicating the successful doping of N. Curve C and D are the FTIR spectra of the samples calcinated at 570 and 700 °C, respectively. The peak at 1210 cm^{-1} disappeared after calcinations due to the N−C═O breakage. The absorption signals in the range 400−1250 cm^{-1} have an obvious shift due to the formation of anatase crystal. To be specific, the pronounced absorption 675 cm^{-1} resulting from the lattice vibrations of TiO_2 shifted to 621 and 584 cm^{-1} because of better crystallization after calcination at 570 and 700 °C, respectively, whereas the peak at 908 cm^{-1} corresponding to asymmetric stretching vibrations of the octahedral [TiO_6] groups shifted to 933 cm^{-1}. Clearly, $H_2Ti_3O_7$ nanosheets are uniformly chemical bonded on the surface of graphene before calcination. The surface modification method used in this study is different from Wen's work, in which the composite is prepared by electrostatic attraction.[31]

3.4. XPS and EDX Analysis. The chemical composition and bonding configuration of nitrogen-doped TiO_2/graphene are demonstrated by the XPS. As observed in Figures 5 and 6,

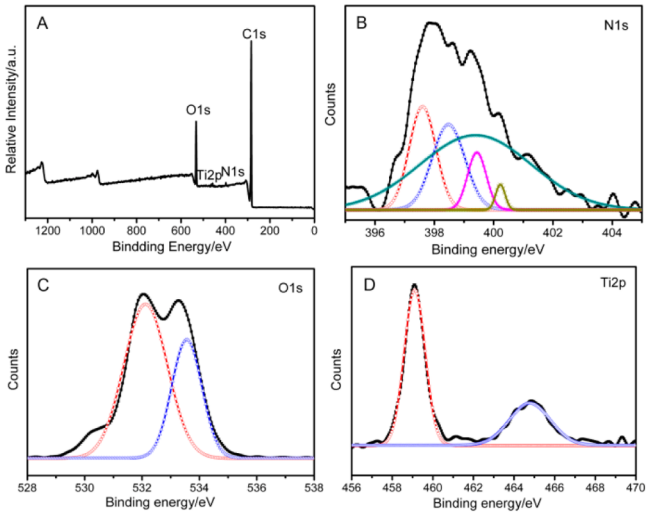

Figure 5. XPS spectra of $H_2Ti_3O_7$/graphene at 570 °C in NH_3 atmosphere for 1 h: (A) survey spectrum; (B) N 1s narrow scan; (C) O 1s narrow scan; (D) Ti 2p narrow scan.

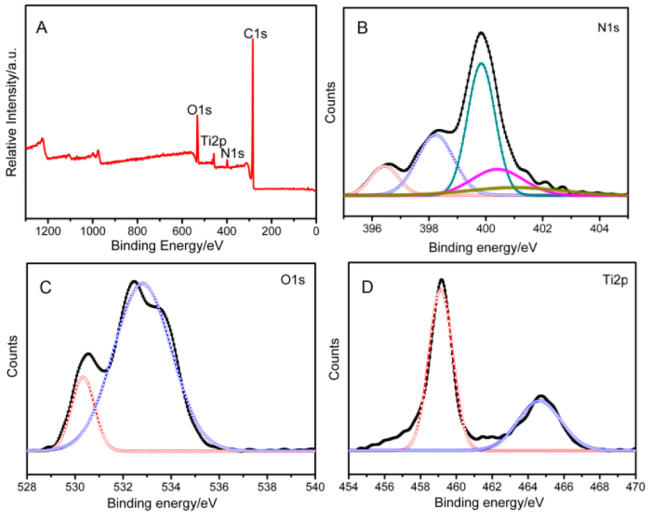

Figure 6. XPS spectra of $H_2Ti_3O_7$/graphene at 700 °C in NH_3 atmosphere for 1 h: (A) survey spectrum; (B) N 1s narrow scan; (C) O 1s narrow scan; (D) Ti 2p narrow scan.

the broad spectrum indicated the existence of C, Ti, O, and N in the composites. Meanwhile, elemental analysis from EDX revealed that 1.56 and 2.78 (atm %) of nitrogen existed in the samples calcined at 570 and 700 °C, respectively (Table 1). It is obvious that higher nitridation temperature can lead to higher nitrogen doping and thus a higher transformation from TiO_2 to TiN. For the sample nitrided at 570 °C, N 1s can be fitted to five peaks, among which the peak at 397.6 eV is ascribed to

Table 1. Relative Atomic Content from EDX Analysis

samples	C (atm %)	N (atm %)	O (atm %)	Si (atm %)	Ti (atm %)
N-TA/G-570	80.54	1.56	13.5	0.70	3.70
N-TA/G-700	76.32	2.78	12.3	1.20	7.40

dx.doi.org/10.1021/am405231p | ACS Appl. Mater. Interfaces 2014, 6, 2118−2124

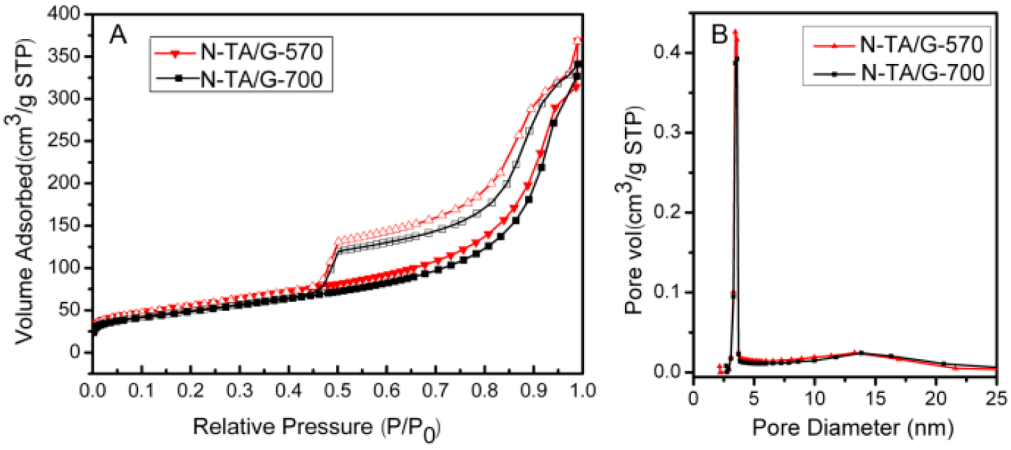

Figure 7. (A) N_2 adsorption and desorption isotherm and (B) pore size distribution of nitrogen-doped TiO_2/graphene nanohybrids.

nitrided N from Ti−N, whereas the other four peaks correspond to C−N (398.5 eV), N_2 (399.37 eV, 399.42 eV), and graphitelike N (400.2 eV), respectively (Figure 5B). In the spectrum of O 1s the broad peak could be fitted into two symmetric peaks at 532.1 and 533.6 eV, which can be attributed to the crystal lattice oxygen (Ti−O−Si) and adsorbed water (H−O−H), respectively (Figure 5C). The peaks at 459.2 and 464.8 eV in the spectrum of Ti 2p can be assigned to Ti ($2P_{3/2}$) and Ti ($2P_{1/2}$), respectively, suggesting that the valence state of Ti was still +4 (Figure 5D). According to the literature,[28,40] the binding energy shifts in the XPS spectra could be explained by the strong interaction (electron transfer) between the nanoscaled semiconductors because of their different Fermi energy levels. When two or more nanoscaled semiconductors bind together, their Fermi energy levels tend to adjust to a same value. That is to say, when the heterojunction is formed, the electron transfer could occur from the semiconductor with higher Fermi energy levels (smaller work function) to the one with lower Fermi energy (larger work function) until the system reaches an equilibrium. As a result, the electron concentration of the semiconductor with higher Fermi energy levels would decrease, which will correspondingly decrease the electron screening effect and result in the enhancement of the binding energy. On the contrary, the electron concentration with lower Fermi energy levels would increase and hence will lead to the decrease of binding energy. Thus, in our case, we believed that the higher binding energy shifts were attributed to the decreased electron concentration of nitrogen-doped TiO_2 nanosheets and increased electron concentration of graphene nanosheets caused by the electron transfer from the nitrogen-doped TiO_2 nanosheets to graphene nanosheets. It is suggested that the work function of the graphene nanosheets may be larger than that of nitrogen-doped TiO_2 nanosheets.

3.5. Specific Surface Area and Pore Size Distribution. In addition, the specific surface areas of nitrogen-doped TiO_2/graphene at 570 and 700 °C are analyzed to be 199 and 174 $m^2 g^{-1}$, respectively, by the Brunauer−Emmett−Teller (BET) method according to N_2 absorption−desorption isotherms as shown in Figure 7A. Clearly, two samples exhibited type IV isotherms with type H1 hysteresis loop according to IUPAC, which are associated with capillary condensation taking place in connected mesopores with similar size.[41,42] The adsorption capacity of sample at 570 °C was slightly larger than that at 700 °C, reflecting an increase in the pore volume at lower nitridation temperature. The hysteresis loops both appearing in a relatively high P/P0 range from 0.5 to 0.9 reveal that the mesopore size is considerably the same. This observation is consistent with the results from the analysis to the pore size distribution (PSD) of products by the BJH method (Figure 7B). Two broad peaks centered at 13.3 and 13.8 nm were observed for the samples nitrided at 570 and 700 °C, indicating that temperature only slightly impacts the pore size of the mixed phase products. The detailed structural information of the products is listed in Table 2. The porous structure and high surface area can provide reactants with more active sites and thus favor the electrochemical activity and the photovoltaic performance of DSSCs.

Table 2. Structural Properties of the Nitrogen-Doped TiO_2/Graphene Obtained from N_2 Adsorption Studies

samples	BET surface area (m^2/g)	pore size (nm)	pore volume (cm^3/g)
N-TA/G-570	199.80	7.69	0.56
N-TA/G-700	174.40	7.75	0.52

3.6. Photovoltaic Performance of the Nitrogen-Doped TiO_2/Graphene. The photocurrent density-photovoltage (J−V) characteristic curves of the DSSCs based on nitrogen-doped TiO_2/graphene at different temperatures as counter electrodes under white light irradiation of 100 mW cm^{-2} are shown in Figure 8A. For comparison, the J−V curves of Pt, undoped TiO_2/graphene and nitrogen-doped TiO_2 were also provided. Apparently, the nitrogen-doped TiO_2/graphene at 700 °C displayed 13% higher short-circuit current density than that of the nitrogen-doped TiO_2/graphene at 570 °C (J_{sc} = 13.7 and 12.4 mA cm^{-2}, respectively). This result is consistent with the EIS analysis. It resulted from the higher nitride content in nitrogen-doped TiO_2/graphene obtained at 700 °C. It is well-known that titanium nitride (TiN) has highly catalytic activity toward the reduction of triiodide ions because of its similarity in the electronic structure with the noble metals. All the photovoltaic parameters derived from the J−V curves have been summarized in Table 3, where it can be noted that the V_{oc} and FF values show remarkable differences depending on the temperature.

Electrochemical impedance spectra (EIS) are also presented to compare the electrochemical behavior between different electrodes prepared at different temperatures. As demonstrated by Nyquist plots (Figure 8B), nitrogen-doped TiO_2/graphene

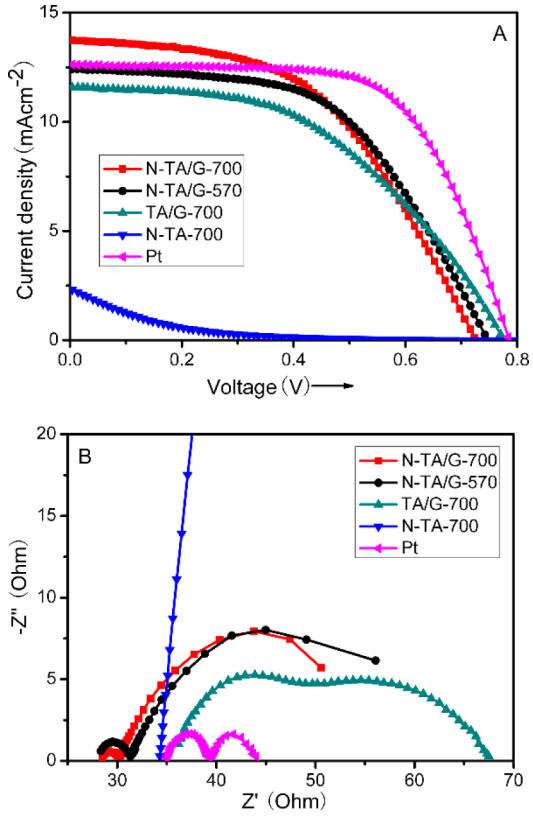

Figure 8. (A) J–V curves for the DSSCs with different counter electrodes at different temperature under AM 1.5 illumination (100 mW cm^{-2}); (B) Nyquist plots for different samples with I^-/I^{-3} redox couple in acetonitrile.

Table 3. Photovoltaic Parameters of DSSCs with Different Counter Electrodes

samples	J_{sc} (mA cm^{-2})	V_{oc} (V)	FF	η (%)
N-TA/G-700	13.73	0.72	0.51	5.04
N-TA/G-570	12.42	0.75	0.54	5.03
TA/G-700	11.58	0.78	0.43	4.44
N-TA-700	2.32	0.70	0.07	0.12
Pt	12.62	0.78	0.64	6.40

[a] V_{oc}, open-circuit voltage. J_{sc}, short-circuit current density. FF, fill factor. η, energy conversion efficiency.

at 700 and at 570 °C electrodes exhibit a semicircle in the high frequency region due to the charge-transfer process at the electrolyte/electrode interface, reflecting their electrocatalytic activity toward I^{3-} reduction. The semicircle diameter of sample nitrided at 700 °C is smaller than that of nitrided at 570 °C, suggesting that the former has a lower charge transfer resistance (R_{ct}) and thus a superior catalytic activity to I^{3-} reduction.

4. CONCLUSIONS

In summary, nitrogen-doped TiO_2/graphene nanohybrids, as highly efficient and low-cost counter electrodes for DSSCs, have been synthesized. It was demonstrated that the mixed-phase nitrided TiO_2 can be formed on the surface after the calcination in ammonia atmosphere for 1 h at 570 and 700 °C, respectively. TEM bright-field image indicated that the nitrogen-doped TiO_2 aggregates were closely embedded within the ultrathin graphene sheets, indicating a successful preparation of nitrogen-doped TiO_2/graphene composites. The nitrogen-doped TiO_2/graphene crystallographic structure was also confirmed by X-ray diffraction with the corresponding diffraction peaks indexed to the cubic anatase phase and the face-centered cubic TiN. XPS and EDX analysis suggested that the higher nitridation temperature would lead to the higher nitrogen elemental content and thus a higher transformation from TiO_2 to TiN. By the photocurrent density-photovoltage test, it was found that the nanohybrids obtained at higher nitridation temperature possessed higher electrocatalytic activity toward I^{3-} reduction when used as counter electrodes in DSCCs, indicating its potential to replace the expensive Pt.

AUTHOR INFORMATION

Corresponding Authors

*E-mail: d.yang@qdu.edu.cn. Tel: 86-532-8595-3361.
*E-mail: jliu@qdu.edu.cn. Tel: 86-532-8595-3361.
*E-mail: ziyanghuo@gmail.com.
*E-mail: x.yao@griffith.edu.au

Notes

The authors declare no competing financial interest.

ACKNOWLEDGMENTS

This work was supported by the National Natural Science Foundation of China (51173087 and 21207073) and Australia Research Council Discovery Project (130104759).

REFERENCES

(1) Jeon, S. S.; Kim, C.; Lee, T. H.; Lee, Y. W.; Do, K.; Ko, J.; Im, S. S. *J. Phys. Chem. C* **2012**, *116*, 22743−22748.
(2) Tian, H.; Yu, Z.; Hagfeldt, A.; Kloo, L.; Sun, L. *J. Am. Chem. Soc.* **2011**, *133*, 9413−9422.
(3) Lin, L.; Nien, P.; Lee, C.; Tsai, K.; Yeh, M.; Vittal, R.; Ho, K. *J. Phys. Chem. C* **2010**, *114*, 21808−21815.
(4) Yang, N.; Zhai, J.; Wang, D.; Chen, Y.; Jiang, L. *ACS Nano* **2010**, *4*, 887−894.
(5) Yang, H.; Guai, G. H.; Guo, C.; Song, Q.; Jiang, S. P.; Wang, Y.; Zhang, W.; Li, C. M. *J. Phys. Chem. C* **2011**, *115*, 12209−12215.
(6) Jeon, S. S.; Kim, C.; Ko, J.; Im, S. S. *J. Phys. Chem. C* **2011**, *115*, 22035−22039.
(7) Wu, J.; Yue, G.; Xiao, Y.; Huang, M.; Lin, J.; Huang, M.; Lin, J.; Fan, L.; Lan, Z.; Lin, J. J. *ACS Appl. Mater. Interfaces* **2012**, *4*, 6530−6536.
(8) Yue, G.; Wu, J.; Xiao, Y.; Lin, J.; Huang, M.; Lan, Z. *J. Phys. Chem. C* **2012**, *116*, 18057−18063.
(9) Fu, N.; Fang, Y.; Duan, Y.; Zhou, X.; Xiao, X.; Lin, Y. *ACS Nano* **2012**, *6*, 9596−9605.
(10) Ameen, S.; Akhtar, M. S.; Kim, Y. S.; Yang, O. B.; Shin, H. *J. Phys. Chem. C* **2010**, *114*, 4760−4764.
(11) Joshi, P.; Zhang, L.; Chen, Q.; Galipeau, D.; Fong, H.; Qiao, Q. *ACS Appl. Mater. Interfaces* **2010**, *2*, 3572−3577.
(12) Dong, P.; Pint, C. L.; Hainey, M.; Mirri, F.; Zhan, Y.; Zhang, J.; Pasquali, M.; Hauge, R. H.; Verduzco, R.; Jiang, M.; Lin, H.; Lou, J. *ACS Appl. Mater. Interfaces* **2011**, *3*, 3157−3161.
(13) Han, J.; Kim, H.; Kim, D. Y.; Jo, S. M.; Jang, S. *ACS Nano* **2010**, *4*, 3503−3509.
(14) Balamurugan, J.; Pandurangan, A.; Thangamuthu, R.; Senthilkumar, S. M. *Ind. Eng. Chem. Res.* **2012**, *52*, 384−393.
(15) Sun, H.; Luo, Y.; Zhang, Y.; Li, D.; Yu, Z.; Li, K.; Meng, Q. *J. Phys. Chem. C* **2010**, *114*, 11673−11679.
(16) Kang, D.; Lee, Y.; Cho, C.; Moon, J. H. *Langmuir* **2012**, *28*, 7033−7038.
(17) Veerappan, G.; Bojan, K.; Rhee, S. *ACS Appl. Mater. Interfaces* **2011**, *3*, 857−862.
(18) Chen, L.; Guo, C. X.; Zhang, Q.; Lei, Y.; Xie, J.; Ee, S.; Guai, G.; Song, Q.; Li, C. M. *ACS Appl. Mater. Interfaces* **2013**, *5*, 2047−2052.

(19) Yao, R.; Zhou, Z.; Hou, Z.; Wang, X.; Zhou, W.; Wu, S. *ACS Appl. Mater. Interfaces* **2013**, *5*, 3143−3148.
(20) Du, Y.; Fan, J.; Zhou, W.; Zhou, Z.; Jiao, J.; Wu, S. *ACS Appl. Mater. Interfaces* **2012**, *4*, 1796−1802.
(21) Zhang, H.; Ge, M.; Yang, L.; Zhou, Z.; Chen, W.; Li, Q.; Liu, L. *J. Phys. Chem. C* **2013**, *117*, 10285−10290.
(22) Shi, J.; Liu, Y.; Peng, Q.; Li, Y. *Nano Research* **2013**, *6*, 441−448.
(23) Zhang, H.; Yu, H.; Han, Y.; Liu, P.; Zhang, S.; Wang, P.; Cheng, Y.; Zhao, H. *Nano Research* **2011**, *4*, 938−947.
(24) Hasin, P.; AlpucheAviles, M. A.; Li, Y.; Wu, Y. *J. Phys. Chem. C* **2009**, *113*, 7456−7460.
(25) Xia, J.; Yuan, C.; Yanagida, S. *ACS Appl. Mater. Interfaces* **2010**, *2*, 2136−2139.
(26) Zhang, Z.; Zhang, X.; Xu, H.; Liu, Z.; Pang, S.; Zhou, X.; Dong, S.; Chen, X.; Cui, G. *ACS Appl. Mater. Interfaces* **2012**, *4*, 6242−6246.
(27) Hao, F.; Lin, H.; Liu, Y.; Wang, N.; Li, W.; Li, J. *ACS Appl. Mater. Interfaces* **2011**, *3*, 3916−3920.
(28) Zhang, Z.; Shao, C.; Li, X.; Sun, Y.; Zhang, M.; Mu, J.; Zhang, P.; Guo, Z.; Liu, Y. *Nanoscale* **2012**, *5*, 606−618.
(29) Peng, S.; Shi, J.; Pei, J.; Liang, Y.; Cheng, F.; Liang, J.; Chen, J. *Nano Res.* **2009**, *2*, 484−492.
(30) Sun, K.; Fan, B.; Ouyang, J. *J. Phys. Chem. C* **2010**, *114*, 4237−4244.
(31) Jiang, Q. W.; Li, G. R.; Liu, S.; Gao, X. P. *J. Phys. Chem. C* **2010**, *114*, 13397−13401.
(32) Jiang, Q.; Li, G.; Gao, X. *Chem. Commun.* **2009**, 6720−6722.
(33) Li, G.; Wang, F.; Jiang, Q.; Gao, X.; Shen, P. *Angew. Chem., Int. Ed.* **2010**, *49*, 3653−3656.
(34) Yang, D. J.; Liu, H. W.; Zhang, Z. F.; Yuan, Y.; Zhao, J. C.; Waclawik, E. R.; Ke, X. B.; Zhu, H. Y. *J. Am. Chem. Soc.* **2009**, *131*, 17885−17893.
(35) Liu, H. W.; Waclawik, E. R.; Zhang, Z. F.; Yang, D. J.; Ke, X. B.; Zhu, H. Y.; Frost, R. L. *J. Phys. Chem. C.* **2010**, *114*, 11430−11434.
(36) Hummers, W. S.; Offeman, R. E. *J. Am. Chem. Soc.* **1958**, *80*, 1339−1339.
(37) Kovtyukhova, N. I.; Ollivier, P. J.; Martin, B. R.; Mallouk, T. E.; Chizhik, S. A.; Buzaneva, E. V.; Gorchinskiy, A. D. *Chem. Mater.* **1999**, *11*, 771−778.
(38) Liu, J. Q.; Wang, R.; Cui, L.; Tang, J. G.; Liu, Z.; Kong, Q. S.; Yang, W. R.; Gooding, J. *J. Phys. Chem. C* **2012**, *116*, 17939−17946.
(39) Wen, Z.; Cui, S.; Pu, H.; Mao, S.; Yu, K.; Feng, X.; Chen, J. *Adv. Mater.* **2011**, *23*, 5445−5450.
(40) Zheng, Y.; Zheng, L.; Zhan, Y.; Lin, X.; Zheng, Q.; Wei, K. *Inorg. Chem.* **2007**, *46*, 6980−6986.
(41) Kruk, M.; Jaroniec, M. *Chem. Mater.* **2001**, *13*, 3169−3183.
(42) Yang, D. J.; Xu, Y.; Wu, D.; Sun, Y. H.; Zhu, H. Y.; Deng, F. *J. Phys. Chem. C* **2007**, *111*, 999−1004.